Linear and nonlinear pulse propagation in a multiple-quantum-well photonic crystal

N. C. Nielsen* and J. Kuhl
Max-Planck-Institut für Festkörperforschung, 70569 Stuttgart, Germany

M. Schaarschmidt, J. Förstner, and A. Knorr
Institut für Theoretische Physik, Technische Universität Berlin, 10623 Berlin, Germany

S. W. Koch
Department of Physics and Material Sciences Center, Philipps-Universität, 35032 Marburg, Germany

G. Khitrova and H. M. Gibbs
Optical Sciences Center, University of Arizona, Tucson, Arizona 85721, USA

H. Giessen
Institute of Applied Physics, University of Bonn, 53115 Bonn, Germany
(Received 21 February 2004; revised manuscript received 26 April 2004; published 16 August 2004)

We investigate the temporal and spectral properties of subpicosecond pulses transmitted on the heavy-hole exciton transition through a multiple-quantum-well Bragg structure, exhibiting a one-dimensional photonic band gap. At low light intensities, a temporal propagation beating is observed. This beating is strongly dependent on the optical dephasing time T_2 which is dominated by the radiative interwell coupling. In an intermediate intensity regime, the Pauli-blocking nonlinearity leads to gradual suppression of the photonic band gap and vanishing of the linear propagation beating. For highly nonlinear excitation, we find signatures of self-induced transmission due to Rabi flopping and adiabatic following of the carrier density. Numerical simulations using the semiconductor Maxwell-Bloch equations are in excellent agreement with the experimental data up to intensities for which higher many-particle correlations become more important and self-phase modulation occurs in the sample substrate.

DOI: 10.1103/PhysRevB.70.075306 PACS number(s): 78.47.+p, 78.20.Bh, 42.50.Md, 78.67.−n

I. INTRODUCTION

The propagation of short laser pulses in layered structures with periodic modulation of the complex susceptibility has attracted wide attention both from a scientific and engineering point of view. The primary goal of research in this area is to modify and control the linear and nonlinear light-matter interaction by tailoring materials and geometric parameters as well as the initial pulse conditions. The most commonly used structure is the dielectric grating made from alternating nonresonant layers. Here, a one-dimensional photonic band gap is formed at the central Bragg wavelength, i.e., twice the optical interlayer distance.[1] Prominent realizations are fiber Bragg gratings[2,3] and integrated Bragg waveguides,[4,5] in which the interplay of the grating dispersion near the photonic band gap with the Kerr-type nonlinearity allows efficient pulse shaping and the propagation of soliton-like pulses. A special class of these Bragg grating solitons are gap solitons that have been predicted for pulses with spectra completely within the band gap.[6,7] Self-induced transparency (SIT) and other forms of soliton solutions were also proposed for resonantly absorbing Bragg gratings, consisting of periodic layers of resonant two-level systems embedded in a homogeneous dielectric medium[8,9] or dielectric grating structure.[10,11]

In this paper, we elucidate the question whether gap solitons are feasible in periodic arrangements of quantum wells (QWs) with an effective interwell spacing equal to half the wavelength of the QW exciton transition. In these multiple quantum well (MQW) Bragg structures, the collective response of the radiatively coupled QWs results in an enhanced radiative decay of the coherent optical polarization.[12,13] The decay time of this superradiant response inversely scales with the QW number N. The reflection from MQW Bragg structures is characterized by a Lorentzian line which grows in peak reflectivity and linewidth with increasing N.[14] In the limit of large N, the reflectivity reaches unity and a square profile characteristic for the reflection of a photonic band gap is formed.[15] Time-resolved reflection experiments and microscopic calculations have shown enhanced emission along with accelerated decay of the coherent optical polarization.[16] At higher excitation intensities, the radiative coupling gradually disappeared, which was attributed to excitation-induced dephasing due to carrier-carrier interaction in the individual QWs. Picosecond partial suppression and full recovery of the photonic band gap associated with MQW Bragg structures was demonstrated recently.[17]

From the resonant propagation of low-intensity pulses through MQWs with *arbitrary* interwell spacing, it is known that those structures may introduce distortions on the transmitted pulse envelope similar to the temporal polariton beating observed in bulk semiconductors.[18–20] These distortions were found to depend on the total thickness of the structure and the dephasing time T_2. Especially when exciting the structure with an intense pump pulse before the arrival of the

 ©2004 The American Physical Society

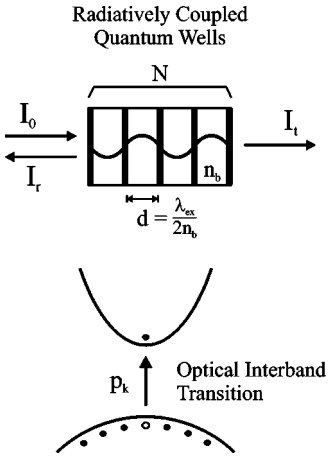

FIG. 1. Schematic picture of the model configuration.

propagating probe pulse—hence, generating an incoherent electron-hole density—the beating could effectively be suppressed. However, the situation is different if the transition from the linear to the nonlinear excitation regime is investigated by an intensity increase of the propagating pulse itself when excitation-induced correlations occur among coherently excited excitons.[21]

In this work, we present a comprehensive analysis of subpicosecond pulse propagation on the lowest heavy-hole exciton transition in a MQW photonic crystal. Our work permits detailed and—with respect to the previously studied reflection geometry—complementary insight into the coherent linear and nonlinear optical response of Bragg-periodic and detuned MQWs. Time- and spectrally resolved measurements are directly compared with theoretical results based on a semiconductor Maxwell-Bloch theory. For linear excitation, we demonstrate a pronounced propagation beating in time. The influence of the radiative interwell coupling and the correspondingly reduced dephasing time T_2 on the pulse propagation characteristics is investigated directly by detuning the structure from the Bragg condition. We show gradual damping of the temporal propagation beating for increasing pulse intensities, for which the relevant Pauli-blocking nonlinearity leads to suppression of the radiative interwell coupling. For highly nonlinear excitation, we find signatures of self-induced transmission due to Rabi flopping and adiabatic following of the carrier density and the occurrence of pulse compression which is predominantly due to self-phase modulation (SPM) in the sample substrate.

II. THEORETICAL MODEL

Our system consists of N equally spaced QWs with separation d which are embedded in a dielectric barrier material with refractive index $n_b=\sqrt{\epsilon}$ (compare Fig. 1). Starting from an input intensity $I_0 \propto |E_0|^2$, the transmitted and reflected intensities $I_{t/r} \propto |E_{t/r}|^2$ are to be determined. Considering linearly polarized light, Maxwell's wave equation for the electric field E reads

$$\left(\partial_z^2 - \frac{1}{c^2}\partial_t^2\right)E = \frac{1}{\epsilon c}\partial_t^2 P_{\mathrm{dyn}} \tag{1}$$

with the nonlinear macroscopic quantum well polarization[12]

$$P_{\mathrm{dyn}}(z) = \sum_n P^n_{\mathrm{dyn}}|\psi_n(z)|^2 = \sum_n \frac{2d_{c,v}}{A}\sum_k p^n_k|\psi_n(z)|^2. \tag{2}$$

Here, ψ_n is the wave function of the nth QW, $d_{c,v}$ is the transition dipole moment, $A=a_0^2$ is the QW area in terms of the exciton Bohr radius a_0, and $p^n_k=\langle \hat{a}^{n\dagger}_{c,k}\hat{a}^n_{v,k}\rangle$ is the wave-number-dependent polarization. Because of the small width of the QWs (typically less than 10 nm) in comparison to the large wavelength of the propagating wave in the MQW structure (more than 200 nm), the square of the wave functions can be approximated as a delta function:[12] $|\psi_n(z)|^2 = \delta(z-z_n)$, where z_n are the QW positions. However, in the numerical calculation, the well width enters as an effective length in the discretization for the finite-difference time-domain (FDTD) algorithm.[22] The material quantities such as the carrier densities and the Coulomb potential are still strictly two dimensional. The Hamiltonian of the semiconductor system can be written as[23]

$$\begin{aligned}\hat{H} = &\sum_{\lambda,k}\varepsilon_{\lambda,k}\hat{a}^\dagger_{\lambda,k}\hat{a}_{\lambda,k} - E\sum_{\lambda\neq\lambda',k} d_{\lambda,\lambda'}\hat{a}^\dagger_{\lambda,k}\hat{a}_{\lambda',k} \\ &+ \tfrac{1}{2}\sum_{\substack{\lambda,\lambda'\\ k,k'\\ q\neq 0}} V_q\hat{a}^\dagger_{\lambda,k+q}\hat{a}^\dagger_{\lambda',k'-q}\hat{a}_{\lambda',k'}\hat{a}_{\lambda,k}\end{aligned} \tag{3}$$

with the carrier creation and annihilation operators $\hat{a}^\dagger_{\lambda,k}$ and $\hat{a}_{\lambda,k}$, the energy eigenvalues $\varepsilon_{\lambda,k}$, and the transition dipole moments $d_{\lambda,\lambda'}$. In the two-band approximation, the treatment is restricted to one valence band v and one conduction band c, i.e., $\lambda,\lambda'=c,v$. We apply the Coulomb matrix element $V_q=e^2/(2\epsilon a_0 A q)$. The equations of motion are derived in Hartree-Fock approximation for the Coulomb interaction:

$$\begin{aligned}\partial_t\tilde{p}^n_k = &-i\omega_k\tilde{p}^n_k + i\tilde{\Omega}^n(1-f^{e,n}_k-f^{h,n}_k) - i\tilde{p}^n_k\sum_{q\neq 0}\frac{V_q}{\hbar}(1-f^{e,n}_{k+q} \\ &- f^{h,n}_{k+q}) + i(1-f^{e,n}_k-f^{h,n}_k)\sum_{q\neq 0}\frac{V_q}{\hbar}\tilde{p}^n_{k+q} - \gamma_0\tilde{p}^n_k\end{aligned} \tag{4}$$

and

$$\partial_t f^{e/h,n}_k = 2Im\left(\tilde{\Omega}^{n*}\tilde{p}^n_k + \tilde{p}^n_k\sum_{q\neq 0}\frac{V_q}{\hbar}\tilde{p}^{n*}_{k+q}\right) - 2\gamma_0 f^{e/h,n}_k, \tag{5}$$

where $f^{e/h,n}_k$ represents the electron and hole distribution functions in the nth QW, $\hbar\omega_k$ are the single-particle energies, $\tilde{\Omega}^n$ is the generalized Rabi frequency, and γ_0 accounts for higher-order many-particle correlations and scattering. The coupled system of the semiconductor Bloch Eqs. (4) and (5) together with Maxwell's wave Eq. (1) are solved directly in time and space using a combined Runge-Kutta and FDTD method.[22] In contrast to previous solutions,[16] this approach allows the treatment of arbitrarily extended samples.

Figure 2(a) shows the linear transmission

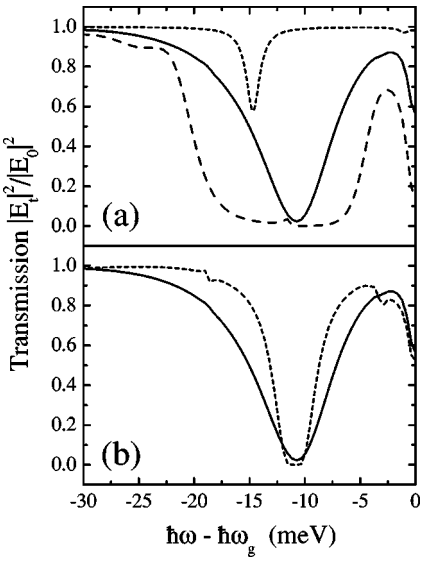

FIG. 2. (a) Linear transmission spectra calculated for Bragg-periodic (In,Ga)As/GaAs MQWs with $N=1$ (short-dashed line), 60 (solid line), and 200 (long-dashed line). (b) Linear transmission spectra calculated for $N=60$ (In,Ga)As/GaAs QWs with $n_b d=0.5\,\lambda_{ex}$ (solid line) and $n_b d=0.475\,\lambda_{ex}$ (short-dashed line).

$$\mathcal{T}=\frac{I_t}{I_0}=\frac{|E_t|^2}{|E_0|^2} \tag{6}$$

calculated for $N=1$, 60, and 200 (In,Ga)As/GaAs QWs with Bragg period $n_b d=0.5\,\lambda_{ex}$, where λ_{ex} is the wavelength of the exciton transition. Here, the (In,Ga)As/GaAs QWs are modeled with an effective well width of 8.5 nm, a dipole matrix element $d_{c,v}=4.2$ eÅ, a refractive index of the barrier $n_b=3.56$, a gap energy $\hbar\omega_g=1.52$ eV, and a phenomenological damping of $\hbar\gamma_0=0.55$ meV. The transmission spectra are dominated by a Lorentzian-shaped extinction line for small QW numbers N. For increasing numbers, this line successively broadens, shifts to higher energies, and grows in peak extinction. Thus, an (In,Ga)As/GaAs MQW Bragg structure with $N=60$ exhibits a minimum transmission at the exciton resonance of $\mathcal{T}=2.2\%$, i.e., an extinction $-\ln(\mathcal{T})=3.8$ with a linear full width at half maximum (FWHM) of 7.7 meV. For QW numbers on the order of $N=100$ and above, the transmission spectrum saturates into a square profile characteristic for a photonic band gap.

The shape and width of the extinction line exhibited by a MQW structure critically depends on the exact fulfillment of the Bragg condition as can be seen in Fig. 2(b). Even slight detuning from $n_b d=0.5\,\lambda_{ex}$ to $0.475\,\lambda_{ex}$ leads to a drastic narrowing of the transmission spectrum. The detuning behavior in combination with the enhanced broadening of the extinction line for an increasing QW number N is a clear manifestation of the collective superradiant response of radiatively coupled QWs and indicates the accelerated decay of the coherent optical polarization. It should be noted that the extinction is mainly of reflective origin for the Bragg-periodic QW arrangement, whereas it is of absorptive nature for the detuned structure.

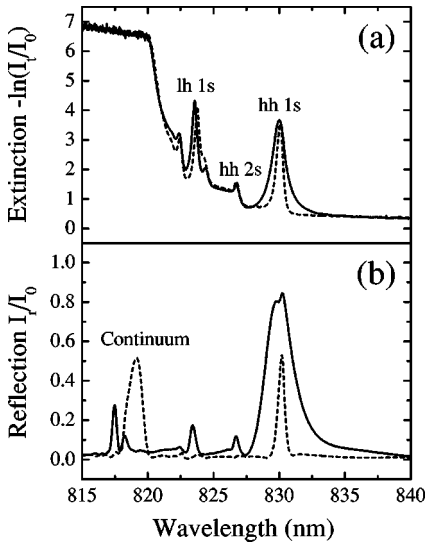

FIG. 3. (a) Linear extinction spectra and (b) linear reflection spectra of the antireflection-coated $N=60$ (In,Ga)As/GaAs MQW structure at $T=9$ K for $n_b d=0.5\,\lambda_{ex}$ (solid line) and $n_b d=0.479\,\lambda_{ex}$ (short-dashed line). Marked are heavy-hole (hh), light-hole (lh), and continuum transitions.

III. SAMPLE AND EXPERIMENTAL TECHNIQUE

A suitable sample structure for investigating pulse propagation phenomena in Bragg-resonant MQWs can be realized in the material system (In,Ga)As/GaAs. The structure should comprise a sufficiently large number of QWs N to provide a long propagation distance and a strong radiative coupling effect while retaining a high sample quality and the required linear transmission. We have epitaxially grown $N=60$ (In,Ga)As/GaAs QWs with 8.5 nm well width and a low indium content of about 4% on a 450-μm-thick GaAs wafer. At $T=9$ K, the heavy-hole (hh) 1s exciton line is situated at $\lambda_{ex}=830$ nm, which is sufficiently far below the GaAs absorption edge (compare Fig. 3). Due to the low refractive index change between the $In_{0.04}Ga_{0.96}$ As QWs and the GaAs barrier material, the reflection caused by the periodic modulation of the real part of the background susceptibility can be neglected. We have additionally coated the front surface of the MQW structure with an antireflection layer. The sample was prepared with a monotonically decreasing barrier thickness from the growth center to the edge of the wafer. Thus, different sample positions correspond to different interwell distances, which allowed us an exact adjustment of the Bragg condition and of any defined detuning in the range from $n_b d=0.505\,\lambda_{ex}$ to $0.470\,\lambda_{ex}$. With $\lambda_{ex}=830$ nm and $n_b(\mathrm{GaAs})\approx 3.65$, Bragg resonance is achieved for $d\approx 113.7$ nm.

Figures 3(a) and 3(b) show the linear extinction $-\ln(\mathcal{T})$ and reflection $\mathcal{R}=I_r/I_0$ of the $N=60$ MQW structure DBR17 at $T=9$ K in Bragg resonance and for the detuned structure with $n_b d=0.479\,\lambda_{ex}$. Clearly observable is the strong broadening of the hh 1s exciton line due to the radiative interwell coupling. The higher exciton and continuum transitions appear as well. For the Bragg-periodic case, the measured extinction at the hh 1s exciton amounts to $-\ln(\mathcal{T})=3.7$, i.e., a

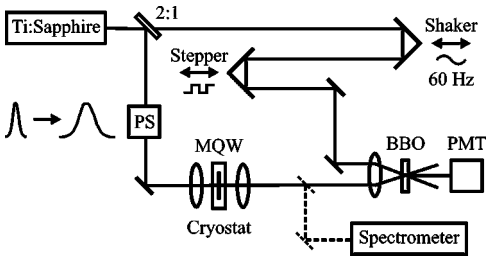

FIG. 4. Experimental setup using high-repetition 100 fs pulses tunable around 830 nm. The shaped and propagated pulses are spectrally recorded and time resolved by cross correlation in a fast-scan sampling scheme. PS: pulse shaper, BBO: β-barium-borate crystal, PMT: photomultiplier tube.

transmission of $\mathcal{T}=2.5\%$ with a linear FWHM of 7.3 meV, which is in accordance with our theoretical model. The predominantly reflective character of the radiatively broadened extinction line becomes obvious when the reflection curves in Fig. 3(b) are compared. Whereas the peak extinction is nearly unchanged for the detuned structure, the peak reflection is reduced, indicating larger absorptive contributions. Superradiant behavior also occurs at the higher transitions and finally at the continuum states when the interwell distance is gradually reduced.[24]

Figure 4 illustrates the experimental setup that is based on a cross-correlation technique. We used 100 fs pulses tunable around 830 nm from a Ti:sapphire oscillator with a repetition rate of 76 MHz. The configuration involves splitting of the linearly polarized laser output into two portions: One part (33%) enters a variable delay line, while the second part (67%) passes through a pulse shaper to tailor 560 fs pulses with sech^2 envelope spectrally matched to the hh 1*s* exciton line. The shaped pulses are focused with a $f=25$ mm microscope objective (Ealing, numerical aperture NA=0.15) onto the MQW sample that is kept at $T=9$ K in a cold-finger cryostat. While the transmitted spectra are directly recorded, the pulses are time resolved by cross correlation with the temporally delayed 100 fs pulses in a 300-μm-thick β-barium-borate crystal cut for type I phase matching. The intensity cross-correlation signal is detected in a photomultiplier tube and may be written as

$$I_c(\tau) \propto \int_{-\infty}^{\infty} I_t(t) I_d(t-\tau) dt, \tag{7}$$

where $I_t(t)$ and $I_d(t)$ are the temporal profiles of the transmitted and delayed pulses, and τ is the pulse delay. We employed a fast-scan sampling technique and averaged over many scans for low-noise pulse acquisition (compare Ref. 25). This technique involves a stabilized shaker system that periodically modulates the pulse delay at a frequency of 60 Hz. A stepper motor is used to produce discrete delay shifts for the time-base calibration.

IV. RESULTS AND DISCUSSION

The results of our pulse propagation experiments and numerical treatment are discussed separately for the linear and nonlinear excitation regimes. First, we describe the propagation of low-intensity pulses through the MQW Bragg structure, the influence of the radiative interwell coupling, and the dependence on the laser detuning from the exciton resonance. In a subsequent section, we investigate the transition from linear to nonlinear pulse propagation and the transmission of high-intensity pulses.

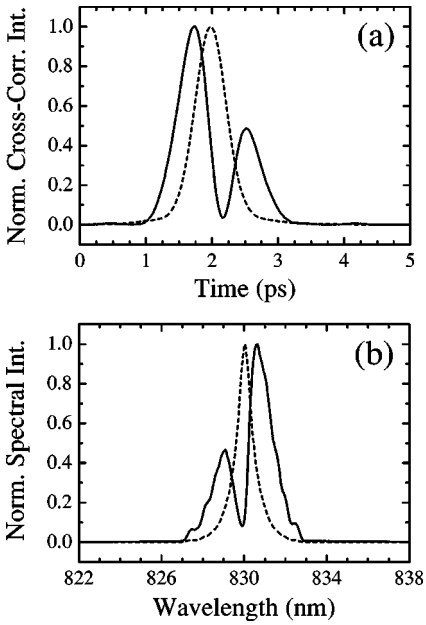

FIG. 5. Propagation of a low-intensity 560 fs input pulse (short-dashed lines) resonant to the hh 1*s* exciton through the Bragg-periodic MQW structure (solid lines). (a) Normalized cross-correlation traces and (b) transmitted spectra.

A. Linear regime

Figure 5 illustrates experimental results of the linear propagation of 560 fs pulses resonantly tuned to the hh 1*s* exciton for Bragg-periodic interwell spacing. The normalized cross-correlation traces of the input (short-dashed lines) and transmitted pulses (solid lines) are plotted for comparison in Fig. 5(a). Note that the input pulse was measured propagating besides the MQW sample with the same experimental configuration and under comparable conditions. For illustration purposes, we subtracted the time delay imposed by the sample. Clearly observable is a pulse splitting into two distinct pulse components separated by approximately 770 fs. The full dip in between appears about 410 fs after the leading pulse peak. Due to the steep edges of the dip, both components exhibit considerable reshaping and narrowing with respect to the input pulse envelope. The corresponding normalized spectra are shown in Fig. 5(b). Here, the pronounced dip in the spectrum transmitted through the sample is caused by the enhanced reflection from the Bragg-coupled QWs and minor absorption contributions.

The linear pulse splitting in the time domain can be explained by interference effects.[26,27] The excitonic resonance is vastly broadened due to superradiant coupling inside the Bragg structure. Cutting out this photonic band gap from the

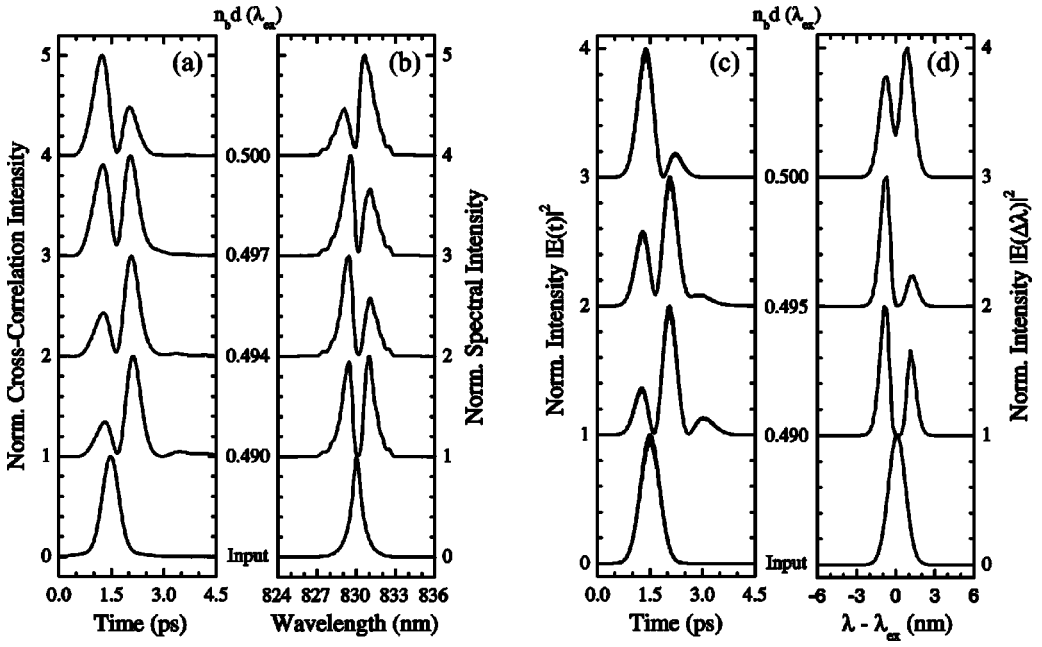

FIG. 6. (a),(b) Propagation of low-intensity 560 fs pulses resonant to the hh 1*s* exciton through the MQW structure for Bragg-periodic and detuned interwell spacing. (a) Normalized cross-correlation traces and (b) transmitted spectra. (c),(d) Numerical simulations based on the semiconductor Maxwell-Bloch equations. (c) Normalized transmitted intensities $|E(t)|^2$ and (d) $|E(\Delta\lambda)|^2$. In experiment and theory, the lowest curves represent the input pulses.

input pulse spectrum leaves two spectral wings propagating freely in the dispersive structure. These two spectral components transform into a propagation beating in time with phase shifts of 180 degrees between the temporal pulse components. Qualitatively, the effect is similar to the polariton propagation beating known from bulk semiconductors.[20,21] However, we find the temporal pulse envelope, especially the amplitude ratio of the two pulse components, to be significantly different from the propagation beating exhibited by MQW structures with comparable length but with an arbitrary interwell spacing.[19] In those structures no photonic band gap is formed because of the lack of superradiant coupling between the individual QWs.

Parameters that critically determine the observed propagation beating are the pulse length τ_p, the optical dephasing time T_2, and the propagation distance Nd. A greater number of Bragg-periodic QWs N will result in a wider photonic band gap, exhibiting a smaller dephasing time T_2. A shorter pulse length τ_p means a larger spectral width of the pulse. If τ_p is short with respect to $T_2/2$ [the optical dephasing time T_2 is defined with respect to the spectral half width at half maximum (HWHM), whereas the pulse length τ_p is defined with respect to the spectral FWHM], a significant amount of spectral components will be transmitted on both sides of the photonic band gap. The interference of these spectral wings during propagation through the dispersive structure will lead to a pronounced temporal beating with several beat periods. On the other side, if τ_p is long with respect to $T_2/2$, almost the entire pulse spectrum will overlap with the photonic band gap. The transmitted pulse will be damped exponentially, and split-off pulse components will be merely weakly pronounced.

The influence of the optical dephasing time T_2 on the pulse propagation characteristics can be studied directly using the wedged design of our MQW sample. Detuning the structure from the Bragg condition weakens the radiative interwell coupling, so that the fast superradiant response of the optical polarization is suppressed, the photonic band gap shrinks, and nonradiative contributions become dominant. In effect, the T_2 time can be tuned from approximately 400 fs for the $N=60$ MQW structure with Bragg period (compare Ref. 14) to a few picoseconds duration for the decoupled QWs. An upper limit of $T_2 \approx 10$ ps for the corresponding (In,Ga)As/GaAs single QWs has been determined from the radiative dephasing rate measured on a series of Bragg structures with different numbers of QWs N (compare Ref. 14) and the nonradiative contributions deduced from the decay of the subradiant modes observed in degenerate four-wave mixing (DFWM) spectroscopy.[24,28]

Figures 6(a) and 6(b) show experimental results of the low-intensity propagation of 560 fs pulses resonant to the hh 1*s* exciton for increasing detuning from the Bragg condition. The temporal cross-correlation traces are plotted in the left column, whereas the right column illustrates the transmitted spectra behind the sample. The lowest curves characterize the input pulse as a reference. All curves have been normalized for comparison. For Bragg-periodic arrangement $n_b d = 0.5\ \lambda_{ex}$ (upper curves in Fig. 6), we find the pulse splitting in time with two pulse components separated by a full coherent dip. In consequence of the enhanced radiative dephasing, the overall pulse envelope declines rapidly after the leading pulse peak so that only one beat period emerges from the coupled QWs. In a phase-sensitive XFROG[29] experiment comparable to Ref. 30, we could also verify the expected phase shift of about 180 degrees between the two pulse components. The observed spectral dip is caused by the asymmetrically broadened reflection from the superradiant

mode. Basically the wings of the input spectrum matched to the resonance are transmitted through the structure. For the gradual reduction of the interwell distance to $n_b d = 0.49\ \lambda_{ex}$ (going from top to bottom in Fig. 6), the measured cross-correlation traces demonstrate considerably altered pulse shapes. Due to the increased T_2 time, the later pulse component successively grows in intensity at the expense of the earlier and becomes dominant already for a slight detuning to $n_b d = 0.497\ \lambda_{ex}$. At $n_b d \approx 0.494\ \lambda_{ex}$ and even more clearly at $n_b d = 0.49\ \lambda_{ex}$, two full beat periods are visible with the three pulse peaks delayed by about 790 and 1290 fs with respect to one another. We did not observe any further change of the pulse envelope for interwell distances below $n_b d = 0.49\ \lambda_{ex}$. As the influence of radiative coupling can almost be neglected in this case, the characteristics are qualitatively similar to the pulse distortions found by Kim *et al.*[19] for subpicosecond pulses transmitted through MQW samples with an arbitrary interwell spacing but with comparable length. The opposite detuning from the Bragg condition to $n_b d > 0.5\ \lambda_{ex}$ showed an analogous propagation behavior with the same strong dependence on the superradiant coupling.

The measured spectra plotted in Fig. 6(b) are characterized by an extinction line that is continuously narrowing with decreasing interwell distance. The transmitted wings of the input spectrum grow in intensity and change their amplitude ratios due to the asymmetric breakdown of the reflection profile starting from the blue edge.[24] The considerably smaller width of the extinction line at $n_b d = 0.49\ \lambda_{ex}$ indicates the suppression of the enhanced radiative polarization decay, which results in an increased dephasing time T_2 and substantial nonradiative contributions.

Results of our numerical simulation are depicted in Figs. 6(c) and 6(d) both temporally and spectrally for a detuning from the Bragg condition to $n_b d = 0.49\ \lambda_{ex}$. The employed semiconductor Maxwell-Bloch theory is capable of describing the observed propagation beating and the dependence on the radiative interwell coupling in excellent agreement with our experimental data. We find the change in the amplitude ratios of the temporal pulse components as well as the development of a second beat period. The calculated delays of the three pulse peaks with respect to one another amount to 780 and 1000 fs, which corresponds to the experimentally determined values. The extinction line, which dominates the spectra, drastically narrows with the detuning to $n_b d = 0.49\ \lambda_{ex}$. Simultaneously, the transmitted spectral wings exhibit an asymmetric growth in intensity that is qualitatively similar to the spectral behavior shown in Fig. 6(b). Our theoretical investigation demonstrates the strong influence of superradiant coupling on the characteristics of subpicosecond pulses propagating resonantly through MQW Bragg structures. Especially, it has been possible to study the impact of a gradually varied dephasing time T_2 in a model system with defined pulse length τ_p and nearly constant propagation distance.

To obtain better insight into the spectral dependencies, we performed linear pulse propagation experiments through the Bragg-periodic MQW structure for different laser detuning around the hh 1*s* exciton resonance $\Delta\lambda = \lambda - \lambda_{ex}$. The temporal and spectral results are shown in Figs. 7(a) and 7(b). As a reference, the lowest curves illustrate the shaped 560 fs input

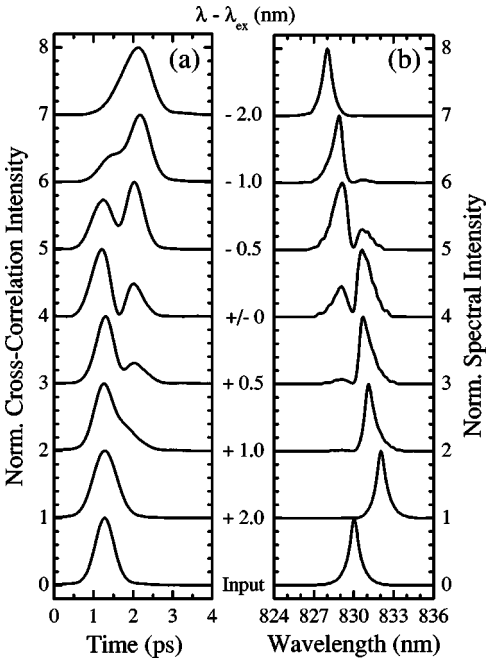

FIG. 7. Propagation of low-intensity 560 fs pulses through the Bragg-periodic MQW structure for different laser detuning around the hh 1*s* exciton resonance. (a) Normalized cross-correlation traces and (b) transmitted spectra. The lowest curves represent the input pulse tuned to resonance.

pulse situated at $\lambda = 830$ nm, i.e., exactly tuned to λ_{ex} at $T = 9$ K. In this case, the spectrum transmitted through the sample is split into two well separated components which exhibit the temporal beating phenomenon with full pulse splitting (see the fifth row from the bottom up in Fig. 7 corresponding to $\Delta\lambda = 0$ nm). Slight detuning of the exciting laser spectrum with respect to the exciton line from $\Delta\lambda = 0$ nm to $\Delta\lambda = \pm 1$ nm leads to a reduced modulation depth in time connected with a severe reshaping of the overall envelope approaching the shape of an individual pulse. In the spectral domain, we observe the enhanced transmission of the respective off-resonant components. Interestingly, an opposite detuning around the exciton line causes the earlier or, conversely, the later pulse component to grow in intensity, which can be ascribed to the different dispersion around the resonance. For larger spectral detuning to $\Delta\lambda = \pm 2$ nm, the temporal modulation is completely suppressed and the corresponding input spectra are restored. However, the transmitted pulses are considerably chirped. This chirp is much more pronounced and accompanied by an additional pulse delay for the spectral detuning to the higher transitions. Our numerical simulations reproduce the suppression of the temporal beating phenomenon for off-resonant excitation in good agreement with the experimental observations (not shown here). A qualitatively similar dependence on the laser detuning is found for the two beat periods emerging from the MQW structure with an interwell spacing deviating from the Bragg condition.

B. Nonlinear regime

In this section, we discuss the transition from linear to nonlinear pulse propagation in MQW Bragg structures.

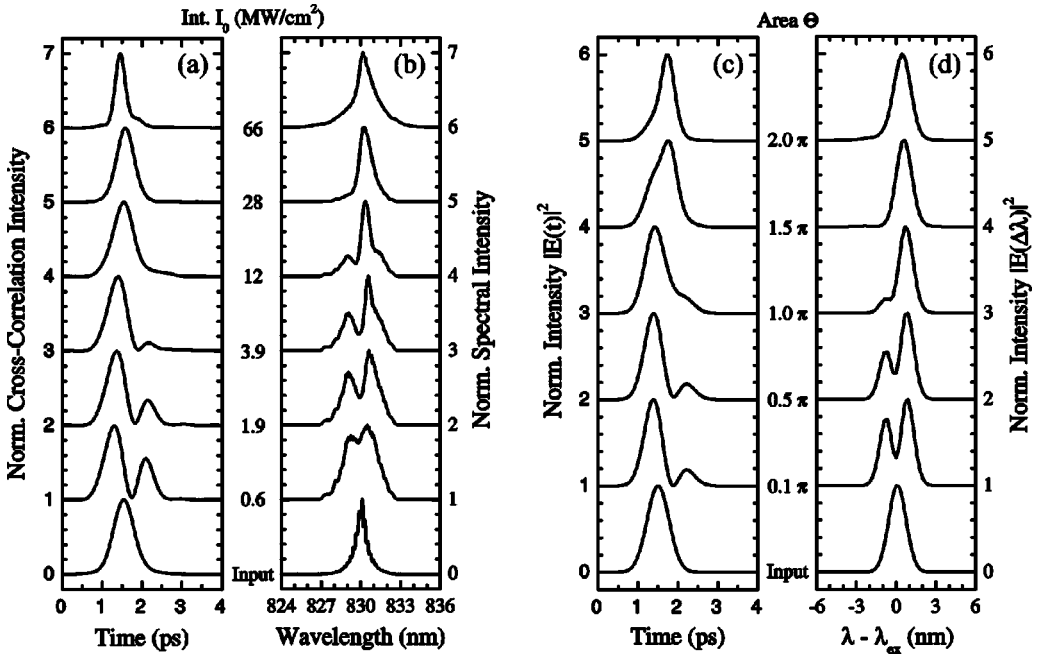

FIG. 8. (a),(b) Propagation of 560 fs pulses resonant to the hh 1*s* exciton through the Bragg-periodic MQW structure for increasing intensities. (a) Normalized corss-correlation traces and (b) transmitted spectra. (c),(d) Numerical simulations based on the semiconductor Maxwell-Bloch equations for increasing pulse area $\Theta \propto \sqrt{I}$. (c) Normalized transmitted intensities $|E(t)|^2$ and (d) $|E(\Delta\lambda)|^2$. In experiment and theory, the lowest curves represent the input pulses.

Within this transition, we describe the damping of the temporal propagation beating and the suppression of the radiative interwell coupling due to the Pauli-blocking nonlinearity. We show signatures of self-induced transmission due to Rabi flopping and adiabatic following of the carrier density.

Figures 8(a) and 8(b) illustrate normalized cross-correlation traces and transmitted spectra measured in Bragg resonance for various excitation intensities I. Again, the lowest curves represent the 560 fs input pulse matched to the hh 1*s* exciton line. The high-frequency modulations in the spectra are caused by the discrete step structure of the reflecting pulse-shaper mask and interferences in the charge-coupled device (CCD) camera of the spectrometer. The linear pulse splitting can be observed up to excitation intensities on the order of MW/cm^2. At $I=0.6$ MW/cm^2, only the pedestal of the incident laser spectrum is transmitted through the sample. The less pronounced extinction line as compared to the previously shown linear spectra is due to the reduced spectral resolution in this measurement series. Increasing the input intensity from 0.6 to 12 MW/cm^2, the curves plotted in Fig. 8(a) exhibit the nonlinear suppression of the temporal propagation beating. The later pulse component successively fades away while the coherent dip within the pulse envelope gradually shifts to later times. Simultaneously, the pulse spectra are more and more governed by a spike growing from the red side of the extinction line [going from bottom to top in Fig. 8(b)]. At an intensity of 28 MW/cm^2, the input pulse is roughly restored in time and spectrum. The total nonlinear transmission has risen up to 33.2% from a linear value of 9.7%. Upon further increase of the intensity to 66 MW/cm^2, the transmitted pulse drastically shortens to about 300 fs FWHM. Connected with this nonlinear pulse compression of almost 50% is a significant distortion of the pulse shape developing modulations on both sides of the temporal peak. The corresponding spectral profile reveals a wide asymmetric broadening in reference to the input spectrum. For the MQW structure detuned from Bragg resonance, we find a qualitatively similar nonlinear behavior with successive damping of the temporal beating phenomenon, pulse restoration, and nonlinear pulse compression.

Results of our numerical simulation are depicted in Figs. 8(c) and 8(d) both temporally and spectrally for increasing pulse area $\Theta=(d_{c,v}/\hbar)\int_{-\infty}^{\infty} E(t)dt$. Here, the temporal integral over the field envelope was chosen as a suitable quantity to measure the pulse strength. For direct comparison of experimental and theoretical curves, note that the intensity goes as pulse area squared: $I \propto \Theta^2$. The semiconductor Maxwell-Bloch theory in Hartree-Fock approximation for the Coulomb interaction reproduces the observed pulse splitting and its gradual suppression for increasing pulse area up to $\Theta=1.0\ \pi$ in agreement with the experimental data. Even the asymmetric spectral behavior with the growing red wing of the transmitted input spectrum is found in the simulation. For pulse areas beyond $\Theta=1.0\ \pi$, the temporal beating phenomenon has completely vanished. However, the envelopes of the propagated pulses plotted in Fig. 8(c) exhibit considerable pulse reshaping: The pulse peak shifts to later times while the initial pulse component declines in intensity. At $\Theta=2.0\ \pi$, the input pulse is compressed from 650 to about 450 fs duration. The associated spectrum reveals a slight redshift and marginal asymmetric broadening.

Comparing experimental and calculated curves in Fig. 8, we find excellent agreement in the propagation behavior of

the pulses with $I=28$ MW/cm^2 and $\Theta=1.5\ \pi$, 12 MW/cm^2 and $1.0\ \pi$, and 3.9 MW/cm^2 and $0.5\ \pi$. With 2.3 and 3.1, the ratios of these intensities roughly correspond to the squared area ratios that amount to 2.25 and 4, respectively. Assuming an intensity of 12 MW/cm^2 for a $1\ \pi$ pulse with $\tau_p=560$ fs, we can give an estimation for the transition dipole moment $d_{c,v}$: Since the measured intensity $I=\frac{1}{2}\sqrt{\epsilon_0/\mu_0}E_0^2$ and the pulse area $\Theta\approx(d_{c,v}/\hbar)E_0\tau_p$, the dipole moment amounts to $d_{c,v}\approx 3.9$ eÅ. This value is in full accordance with the dipole moment $d_{c,v}=4.2$ eÅ used for the simulations and literature values for GaAs ranging from $d_{c,v}\approx 3$ to 6 eÅ.[31]

The transition from the resonant linear to nonlinear pulse propagation can be explained by the Pauli-blocking nonlinearity. For an input pulse with area $\Theta\leqslant 1.0\ \pi$, the reflection from the effective photonic band gap together with the absorptive contributions cause a splitting of the transmitted spectrum into two portions. The corresponding Fourier transforms yield a beating phenomenon in time. Initially, the temporal duration of the pulse is longer than the response time of the MQW Bragg structure. Therefore, the pulse-induced temporal dynamics are quasistationary and the population follows the pulse envelope adiabatically. Due to the Pauli-blocking nonlinearity, further interband transitions are prevented. Thus, for an increasing pulse area towards $\Theta=1.0\ \pi$, the dip in the transmitted spectrum is filled up and the temporal beating phenomenon gradually vanishes. As Pauli blocking leads to a decoupling of the QW polarization from the propagating light field [the light interaction term $+i\tilde{\Omega}^n(1-f_k^{e,n}-f_k^{h,n})$ in Eq. (4) is reduced for increasing carrier densities $f_k^{e/h,n}$], the effective interwell coupling decreases, starting at the first QW. In consequence, the photonic band gap is suppressed but quickly recovers after the pulse transit because of radiative decay of the population inversion.[17] Thus, for pulse areas $\Theta>1.0\ \pi$, the pulse transmitted through the structure will have a temporal shape and spectrum more similar to the input characteristics. The deviations, such as time delay and shortening with respect to the incident pulse, can be explained as follows: During the propagation there is a temporally delayed interchange of energy between the pulse and the excitonic system, i.e., excitation and reemission (decay and reestablishment of the band gap). This interchange causes the temporal pulse delay. As the breakdown and recovery of the band gap appears instantaneously with a higher-order nonlinearity, temporal steepening and shortening of the transmitted pulse is observed. Of course, many-body interaction in the semiconductor system will cause deviations from this idealized description. Despite the similarity of input and transmitted pulses, pure solitons such as SIT solitons (known from the dynamics of two-level systems) or gap solitons are not expected in such a semiconductor system. Nevertheless, Rabi flopping of the carrier density, coherent nonlinear long-distance propagation, and a high degree of this so-called self-induced transmission have been predicted[32,33] and shown recently for bulk semiconductors.[25,34]

To highlight the difference between the dynamics of two-level systems and the MQW photonic crystal, Fig. 9 illustrates the band-gap dynamics and carrier-density Rabi flopping in the semiconductor material. The densities $(1/A)\Sigma_k f_k^{e/h}(t)$ in the final QW of the Bragg-periodic MQW structure are plotted with respect to the corresponding input and transmitted field envelopes. For an input pulse area of $\Theta=2.0\ \pi$ [Fig. 9(a)], the carrier density follows the input pulse instantaneously, similar to a single Rabi cycle, which here, however, is due to breakdown and recovery of the photonic band gap.[17] For an area of $\Theta=10\ \pi$ [Fig. 9(b)], we observe on top of the band-gap dynamics five distinct Rabi oscillations of the carrier density. Clearly visible are several modulations of the transmitted pulse envelope that reach their maxima shortly after the peak densities, i.e., shortly after the onset of the coherent nonlinear reemission from the final QW. Multiple pulse breakup, which is well known from coherent nonlinear pulse propagation in optically thick bulk semiconductors,[25,34] does not develop during propagation through $N=60$ QWs. However, the results are in good agreement with pump-probe experiments performed on MQWs with arbitrary interwell spacing (compare Ref. 35).

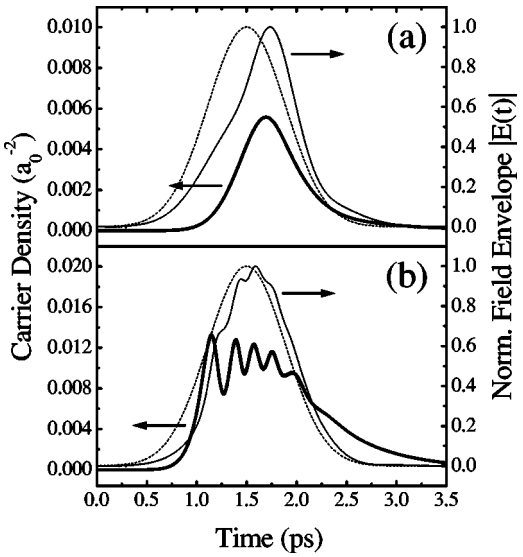

FIG. 9. Carrier densities in the 60th QW (thick solid lines) and normalized field envelopes of the resonant 650 fs input (thin dashed lines) and transmitted pulses (thin solid lines) calculated for the Bragg-periodic MQW structure. (a) $\Theta=2.0\ \pi$ and (b) $\Theta=10\ \pi$.

The experimental and theoretical results of the highly nonlinear propagation through the Bragg-resonant MQW structure are plotted in Fig. 10 with respect to the 560 fs input pulse profiles. Pulse reshaping and compression due to a single Rabi cycle and adiabatic following of the carrier density at $\Theta=2.0\ \pi$ can clearly be seen in Fig. 10(c). The corresponding spectrum equals the input spectrum in shape apart from a slight redshift and asymmetric broadening towards the blue edge [compare Fig. 10(d)]. The much stronger pulse compression, the temporal modulations, and above all the wide spectral broadening found in the experiment for the highest pulse intensity of $I=66$ MW/cm^2 [Figs. 10(a) and 10(b)] could not be reproduced by our theoretical approach. We explain this deviation by the contribution of many-particle correlations beyond Hartree-

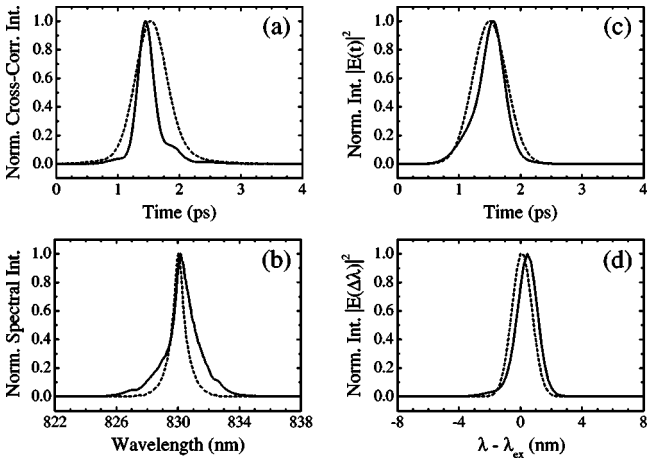

FIG. 10. High-intensity propagation of 560 fs input pulses (short-dashed lines) resonant to the hh 1*s* exciton through the Bragg-periodic MQW structure (solid lines). (a) Normalized cross-correlation traces and (b) transmitted spectra. (c) Normalized calculated intensities $|E(t)|^2$ and (d) $|E(\Delta\lambda)|^2$.

Fock levels and the additional contribution of near-resonant SPM in the GaAs substrate material.[36] Tuning the laser wavelength around the QW exciton transition as well as experiments performed on bulk GaAs showed similar nonlinear effects, thus giving proof for the strong influence of SPM.

The results presented in this section provide evidence for self-induced transmission due to Rabi oscillations on the hh 1*s* exciton resonance and adiabatic following of the carrier density. In agreement with earlier investigations, this finding demonstrates that even for excitation intensities in the range of tens of MW/cm^2, substantial coherence between the exciting laser field and the excitonic polarization within the individual QWs is maintained over several hundred femtoseconds. However, superradiant interwell coupling plays a minor role in this nonlinear excitation regime, so that the propagation through the MQW Bragg structure becomes qualitatively similar to the propagation through a MQW structure with arbitrary interwell spacing or even a thin film of bulk semiconductor material.

V. CONCLUSIONS

We have presented an experimental and theoretical study of subpicosecond pulse propagation on the lowest heavy-hole exciton transition in an extended MQW Bragg structure, exhibiting a one-dimensional photonic band gap. In the linear regime, a pronounced temporal propagation beating emerges from the interference of spectral components transmitted on both sides of the radiatively broadened exciton resonance. This propagation beating is highly sensitive to the radiative interwell coupling, which clearly demonstrates the influence of the optical dephasing time T_2 on the coherent propagation of low-intensity pulses. The transition from linear to nonlinear excitation manifests itself in a gradual damping of the temporal beating phenomenon. In this regime, the Pauli-blocking nonlinearity leads to a decoupling of the QW polarization from the propagating light field so that the radiative interwell coupling is suppressed and the photonic band gap breaks down. Gap solitons cannot be expected in such a MQW photonic crystal. For highly nonlinear excitation, the reshaped input pulses are transmitted through the structure, and we find signatures of self-induced transmission due to Rabi flopping and adiabatic following of the carrier density. Numerical simulations using the semiconductor Maxwell-Bloch equations in Hartree-Fock approximation for the Coulomb interaction are in excellent agreement with the experimental data up to intensities for which higher many-particle correlations become more important and SPM occurs in the sample substrate.

ACKNOWLEDGMENTS

The authors would like to thank H.-U. Habermeier and F. Schartner for the fabrication of the pulse-shaper masks. Financial support for the Berlin group came especially from the Deutsche Forschungsgemeinschaft through the Sonderforschungsbereich "Wachstumskorrelierte Eigenschaften niederdimensionaler Halbleiterstrukturen." S. W. K. thanks for financial support through the DFG photonic crystal program and the Humboldt Foundation and the Max Planck Society for support through the Max Planck Research Prize. The Tucson group thanks NSF (AMOP and EPDT) and JSOP (AFOSR and ARO). H. G. thanks the DFG for support through their program SPP 1113 and the BMBF "Photonic Crystal" program.

*Electronic address: n.nielsen@fkf.mpg.de

[1] L. Brillouin, *Wave Propagation in Periodic Structures* (McGraw-Hill, New York, 1946).
[2] H. G. Winful, Appl. Phys. Lett. **46**, 527 (1985).
[3] B. J. Eggleton, R. E. Slusher, C. M. de Sterke, P. A. Krug, and J. E. Sipe, Phys. Rev. Lett. **76**, 1627 (1996).
[4] P. Millar, R. M. de la Rue, T. F. Krauss, J. S. Aitchison, N. G. R. Broderick, and D. J. Richardson, Opt. Lett. **24**, 685 (1999).
[5] N. G. R. Broderick, P. Millar, D. J. Richardson, J. S. Aitchison, R. de la Rue, and T. Krauss, Opt. Lett. **25**, 740 (2000).
[6] W. Chen and D. L. Mills, Phys. Rev. Lett. **58**, 160 (1987).
[7] A. B. Aceves and S. Wabnitz, Phys. Lett. A **141**, 37 (1989).
[8] B. I. Mantsyzov and R. N. Kuz'min, Sov. Phys. JETP **64**, 37 (1986).
[9] B. I. Mantsyzov, Phys. Rev. A **51**, 4939 (1995).
[10] A. Kozhekin and G. Kurizki, Phys. Rev. Lett. **74**, 5020 (1995).
[11] A. E. Kozhekin, G. Kurizki, and B. Malomed, Phys. Rev. Lett. **81**, 3647 (1998).
[12] T. Stroucken, A. Knorr, P. Thomas, and S. W. Koch, Phys. Rev. B **53**, 2026 (1996).

[13] M. Hübner, J. Kuhl, T. Stroucken, A. Knorr, S. W. Koch, R. Hey, and K. Ploog, Phys. Rev. Lett. **76**, 4199 (1996).
[14] J. P. Prineas, C. Ell, E. S. Lee, G. Khitrova, H. M. Gibbs, and S. W. Koch, Phys. Rev. B **61**, 13863 (2000).
[15] J. Förstner, K. J. Ahn, J. Danckwerts, M. Schaarschmidt, I. Waldmüller, C. Weber, and A. Knorr, Phys. Status Solidi B **234**, 155 (2002).
[16] S. Haas, T. Stroucken, M. Hübner, J. Kuhl, B. Grote, A. Knorr, F. Jahnke, S. W. Koch, R. Hey, and K. Ploog, Phys. Rev. B **57**, 14860 (1998).
[17] J. P. Prineas, J. Y. Zhou, J. Kuhl, H. M. Gibbs, G. Khitrova, S. W. Koch, and A. Knorr, Appl. Phys. Lett. **81**, 4332 (2002).
[18] D. S. Kim, J. Shah, D. A. B. Miller, T. C. Damen, W. Schäfer, and L. Pfeiffer, Phys. Rev. B **48**, 17902 (1993).
[19] D. S. Kim, J. Shah, D. A. B. Miller, T. C. Damen, A. Vinattieri, W. Schäfer, and L. N. Pfeiffer, Phys. Rev. B **50**, 18240 (1994).
[20] D. Fröhlich, A. Kulik, B. Uebbing, A. Mysyrowicz, V. Langer, H. Stolz, and W. von der Osten, Phys. Rev. Lett. **67**, 2343 (1991).
[21] J. Förstner, A. Knorr, S. Kuckenburg, T. Meier, S. Koch, H. Giessen, S. Linden, and J. Kuhl, Phys. Status Solidi B **221**, 453 (2000).
[22] R. W. Ziolkowski, J. M. Arnold, and D. M. Gogny, Phys. Rev. A **52**, 3082 (1995).
[23] H. Haug and S. W. Koch, *Quantum Theory of the Optical and Electronic Properties of Semiconductors* (World Scientific, Singapore, 1994).
[24] D. Ammerlahn, J. Kuhl, B. Grote, S. W. Koch, G. Khitrova, and H. Gibbs, Phys. Rev. B **62**, 7350 (2000).
[25] N. C. Nielsen, S. Linden, J. Kuhl, J. Förstner, A. Knorr, S. W. Koch, and H. Giessen, Phys. Rev. B **64**, 245202 (2001).
[26] M. D. Crisp, Phys. Rev. A **1**, 1604 (1970).
[27] J. M. Friedmann, H. M. Gibbs, T. N. C. Venkatesan, B. Bölger, D. Polder, and M. F. H. Schuurmans, Opt. Commun. **20**, 183 (1977).
[28] J. Kuhl *et al.*, in *Festkörperprobleme/Advances in Solid State Physics*, edited by B. Kramer (Vieweg, Braunschweig, 1999), Vol. 38, p. 281.
[29] S. Linden, H. Giessen, and J. Kuhl, Phys. Status Solidi B **206**, 119 (1998).
[30] Y. Mitsumori, R. Kawahara, T. Kuroda, and F. Minami, J. Lumin. **94–95**, 645 (2001).
[31] O. D. Mücke, T. Tritschler, M. Wegener, U. Morgner, and F. X. Kärtner, Phys. Rev. Lett. **87**, 057401 (2001).
[32] R. Binder, S. W. Koch, M. Lindberg, N. Peyghambarian, and W. Schäfer, Phys. Rev. Lett. **65**, 899 (1990).
[33] S. W. Koch, A. Knorr, R. Binder, and M. Lindberg, Phys. Status Solidi B **173**, 177 (1992).
[34] H. Giessen, A. Knorr, S. Haas, S. W. Koch, S. Linden, J. Kuhl, M. Hetterich, M. Grün, and C. Klingshirn, Phys. Rev. Lett. **81**, 4260 (1992).
[35] A. Schülzgen, R. Binder, M. E. Donovan, M. Lindberg, K. Wundke, H. M. Gibbs, G. Khitrova, and N. Peyghambarian, Phys. Rev. Lett. **82**, 2346 (1999).
[36] P. A. Harten, A. Knorr, J. P. Sokoloff, F. B. de Colstoun, S. G. Lee, R. Jin, E. M. Wright, G. Khitrova, H. M. Gibbs, S. W. Koch, and N. Peyghambarian, Phys. Rev. Lett. **69**, 852 (1992).